Using Remote Sensing to Understand the Total Suspended Matter Dynamics in Lakes Across Inner Mongolia

Yunxia Du, Kaishan Song ⓘ, Qiang Wang, Ge Liu, Zhidan Wen, Yingxin Shang, Lili Lyu, Jia Du, Sijia Li, Hui Tao, Baohua Zhang, and Xiang Wang

Abstract—An exponential function model was developed based on the red band from Landsat and *in situ* data. The model performed well, the calibration determination coefficient (R^2) was 0.82 and validation metrics root-mean-square error, mean absolute percent error, and bias was 8.23 mg/L, 30% and -2.35 mg/L, respectively. Then, the time series of total suspended matter (TSM) concentrations for the lakes across Inner Mongolia were presented using the Landsat data from 1984–2019. The results showed that the number of the lakes with TSM decrease was slightly more than that with TSM increase (57% versus 43%). A total of 70.72% of those lakes had a changing rate less than 1 mg/L/yr in TSM, while the other 29.28% had a changing rate more than 1 mg/L/yr. In some lakes (24.2%), the coefficient of variation was greater than 102% indicating significant spatial variation. The TSM less than 20 mg/L mainly appeared in the reservoirs. Based on different environmental backgrounds, this study showed comprehensive estimates (increasing and decreasing regions) of TSM concentrations. Finally, the relative roles of several factors to the TSM changes were quantified and examined at different scales. The responses of TSM changes to NDVI representing vegetation coverage indicated that vegetation played an important role for most lakes. Whilst wind speed and precipitation significantly affected a few lakes. For most lakes, the TSM were affected by multiple factors, where a single factor could not be highlighted. Nevertheless, a comprehensive analysis of the factors surrounding a lake remains relevant for determining the possible trend (better or worse) of its TSM variation.

Yunxia Du is with the Northeast Institute of Geography and Agroecology, Chinese Academy of Sciences, Changchun 130102, China, and also with the University of Chinese Academy of Sciences, Beijing 100049, China (e-mail: duyunxia@iga.ac.cn).

Kaishan Song is with the Northeast Institute of Geography and Agroecology, Chinese Academy of Sciences, Changchun 130102, China, and also with the School of Environment and Planning, Liaocheng University, Liaocheng 252000, China (e-mail: songkaishan@iga.ac.cn).

Qiang Wang, Ge Liu, Zhidan Wen, Yingxin Shang, Lili Lyu, Jia Du, Sijia Li, Hui Tao, and Xiang Wang are with the Northeast Institute of Geography and Agroecology, Chinese Academy of Sciences, Changchun 130102, China (e-mail: 15590287488@163.com; liuge@iga.ac.cn; wenzhidan@iga.ac.cn; shangyingxin@iga.ac.cn; lvlili@iga.ac.cn; jiaqidu@neigae.ac.cn; lisijia@iga.ac.cn; taohui@iga.ac.cn; wangxiang5690@outlook.com).

Baohua Zhang is with the School of Environment and Planning, Liaocheng University, Liaocheng 252000, China (e-mail: zhangbaohua@lcu.edu.cn).

I. Introduction

THE major inland water resources, such as lakes, reservoirs and rivers, are important to support domestic, industrial and agricultural consumptions [1]. However, these inland lakes (lakes include 324 reservoirs and 267 natural lakes in this study) are under pressure due to human interference and climate change [2], [3]. Driven by concerns about water scarcity challenges in the future, the study of water quality is becoming more important in many countries [4], [5]. It is imperative to prevent and manage water pollution, and collect reliable water quality data. The total suspended matter (TSM) is an important water quality parameter which is commonly used for water quality evaluation, especially for inland lakes. It determines the transparency of water, and ultimately reflects the primary productivity of water [6]. High TSM concentration is generally expected to cause habitat deterioration for the benthic zone [7]. In this sense, it is essential to monitor TSM concentration in order to understand the physical, chemical, biological and environmental processes and their interrelationships in aquatic systems [8]. It is co-determined by various environmental variables in the lakes and catchment [9].

The application of remote sensing techniques can facilitate the dynamic monitoring of TSM concentration to better interpret the water quality status. Since the late 1970s, a wide variety of operational ocean color satellite sensors and algorithms have been developed and optimized continuously for the inland lakes and the ocean [10], [11]. Meanwhile, some satellite missions were designed for land applications, they also sparked a new interest from the water quality remote sensing community for high resolution imagery [12], [13], especially the Landsat satellite series [14], [15]. With much higher spatial and temporal coverages than the conventional sampling methods, these remote sensing sensors combined with corresponding algorithms have been applied for tracking several environmental processes [16], and for estimating some water quality parameters including water clarity and TSM [17]–[19]. From the long-term satellite data, the expected behavior and the natural variability of the investigated signal can be identified at pixel level [20]. Nevertheless, due to the complex optical characteristics of turbid inland

lakes, limitations of the algorithms used with the multispectral ocean color sensors are still present in existing studies [10], [19]. It is a technical challenge to address the severe limitation of these algorithms in inland lakes and refine their detection limits in various aquatic environments.

Remote sensing retrieval of inland water quality is based on the assumption that the relationship between the reflectance and the concentration of water quality constituents is known *a priori* [21]. The application of satellite remote sensing for water quality assessment and monitoring requires accurate water reflectance received from the water in order to retrieve reliable water quality parameters [17]. However, signals reaching a sensor above water are often weakened by the undesired atmospheric effects caused by absorption and scattering [22]. Thus, the atmospheric correction that can remove such undesired effects from sensor received signals, is a crucial procedure for inland lakes quality monitoring [23]. This challenging task has motivated scientists to develop numerous atmospheric correction methods for estimating water quality parameters of inland lakes [24], [25]. However, a generic, automated and reliable atmospheric correction tool has not been developed for water applications of multispectral sensor data at present [13]. In view of this situation, the surface reflectance from United States Geological Survey (USGS) (https://www.usgs.gov/) is preferred in several cases. The USGS data improve the comparison between multiple images over the same region by accounting for atmospheric effects (such as aerosol scattering and thin clouds) which can help in the detection and characterization of earth surface change (https://www.usgs.gov/).

There have been several researches on water transparency in larger lakes across Inner Mongolia. The water transparency in several lakes with the area >20 km^2 during 2000-2018 were retrieved by Liu *et al.* [52]. Song *et al.* [53] mapped water transparency in the lakes with area >8 ha with OLI images mainly acquired in 2016. The spatial characteristics of water transparency between 2016 and 2018 were detected by Zhang *et al.* [54] using Landsat 8 images for lakes with area ≥10 km^2. In contrast, TSM remote sensing research on a long-term scale has not been reported for Inner Mongolia. The long-term historical data from Landsat may provide an invaluable archive for the TSM dynamic study. This article has three key objectives. First, we tested and evaluated the Landsat data by regression analysis to retrieve the TSM in the inland lakes of the study area. Second, we mapped the spatiotemporal dynamics of the TSM concentrations across the study area using the robust model for identifying the areas of persistently elevated TSM concentrations (which might experience serious water quality issues). Third, the correlations between TSM variations and factors (NDVI, wind speed and precipitation) were explored for the implementation of water quality management.

II. MATERIALS AND METHODS

A. Study Area

Inner Mongolia, located in the northern border of China in Eurasia (see Fig. 1), has a population of 25.048 million. It has a vast territory with a straight-line distance of 2400 km from west to east, and a span of 1700 km from south to north. The elevation
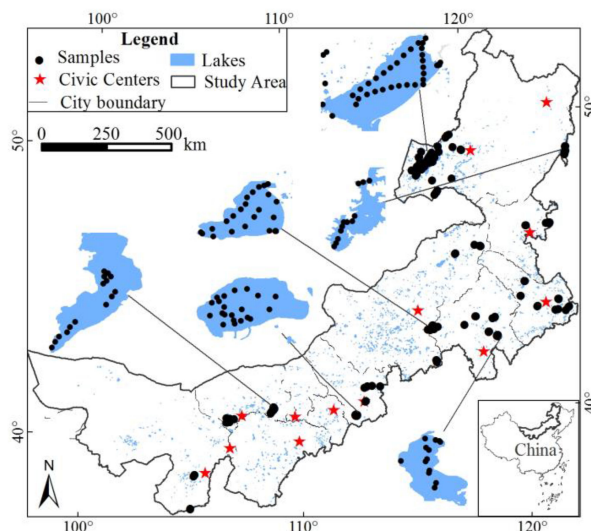

Fig. 1. Information of study area and samples.

of most areas in this region is above 1000 meters, and this region mainly shows plateau landforms. Since this region is far from the ocean and blocked by mountains on the edge, the climate of this region is mainly characterized by a temperate continental monsoon climate with low and uneven precipitation (a total annual precipitation of 50–450 mm), strong winds (average annual wind speed above 3 m/s), and huge temperature variation (the difference of average annual temperature is 34 °C –36 °C and average daily temperature is 12 °C –16 °C). The ground surface is mainly covered by grassland (86.667 million hectares), forest (20.8 million hectares), farmland (5 491 400 hectares of usable arable land) and desert. Among them, the areas of grassland and forest are the largest in China.

Inner Mongolia is one of the driest provinces in China, and the total amount of water resources is 50.922 billion m^3 accounting for 1.86% of the total amount of water resources in China [26]. Moreover, the amount of water resources allocated per capita and per land is small. The distributions of water resources and population or arable land are uneven. In particular, affected by factors such as natural geographic location and topography, the distribution of water resources in Inner Mongolia is extremely uneven among regions or in interyears and intrayear. Consequently, the strategic layout of economic and social development for Inner Mongolia is very much restricted [26]. The TSM in the lakes with an area greater than 0.1 km^2 was retrieved and the time series with TSM of more than ten years were further analyzed in this article.

B. Samples and TSM Measurements

In this article, the water samples were collected in the field. Several lakes located in different geographical regions (see Fig. 1) were sampled one to two times each year over a period of six years (2013–2015, 2017–2019) in order to make the TSM concentration retrieval model robust and extensible. The minimum distance between sampling points in the same period was 500 m. The geographic location of each point was recorded using DGPS-Pomark2 (UniStrong company, Beijing,

China) (see Fig. 1). Water samples were gathered and stored in amber-colored 1-L HDPE bottles. At each sampling point, approximately 2 L of water were collected at 0.1–1 m below the water surface. All samples were kept in a portable refrigerator at 4°C and dark environment before they arrived at laboratory. A total of 216 samples were collected (see Fig. 1).

In the laboratory, samples were filtered in amounts of 150–200 mL through preashed, preweighed 47 mm diameter, 0.7 μm pore size glass fiber filters. The sample filters were dried at 100°C and then placed in a desiccator to cool down. The filters were weighed using a 0.0001 g resolution scale before and after filtration. The TSM concentration was calculated based on the sediment in the filters and the water volume used for filtration.

C. Remote Sensing Data Selection and Model Development

We applied the Landsat surface reflectance data generated by the Landsat Ecosystem Disturbance Adaptive Processing System (LEDAPS) (version 3.4.0) or Land Surface Reflectance Code (LaSRC) (version 1.4.1) algorithm from USGS in this article. The surface reflectance data accounted for atmospheric effects, such as aerosol scattering and thin clouds (https://www.usgs.gov/). First, we obtained the synchronous or quasi-synchronous (within ten days) Landsat surface reflectance data for the samples. A total of 115 pairs of in situ measured TSM and Landsat images were acquired (see Table S1). Next, we extracted the reflectance at each sampling point from the matched Landsat surface reflectance data by importing the latitude and longitude values.

After that, all 115 sample pairs were randomly divided into two data sets, of which two-thirds (77) were used as calibration data set for model calibration and one-third (38) were used as validation data set for model validation. We correlated the TSM sample measurements with the corresponding reflectance values of each band (blue, green, red, and NIR) or band combination (two-bands combinations and three-bands combinations among blue, green, red, and NIR) from Landsat images at each sampling point. According to the relationship between TSM and reflectance displayed by the statistical analysis software, we could identify the relatively sensitive band or combination. Finally, the models were fitted by regression analysis (linear, polynomial, exponential, power and logarithmic) using the sensitive band or combination.

The models were validated with the mean absolute percent error (MAPE), root mean square error (RMSE), and bias. The determination coefficient (R^2) for model calibration, the metrics for validation (MAPE, RMSE, and bias), and the scatter plot of the validation data along the 1:1 line were compared and analyzed to assess the models. The model performed best was further used for TSM retrieval. The formulas for these model accuracy evaluation metrics are as follows:

$$\text{RMSE} = \sqrt{\frac{\sum_{i=1}^{n}(x_i - x_i')^2}{n}} \tag{1}$$

$$MAPE = \frac{\sum_{i=1}^{n}\left|\frac{x_i - x_i'}{x_i}\right|}{n} \times 100\% \tag{2}$$

$$\text{bias} = \frac{\sum_{i=1}^{n}(x_i' - x_i)}{n} \tag{3}$$

where x_i is the observed value of ith element, x_i' is the estimated value of ith element and n is the number of elements.

D. Time Series TSM Map Generation

Based on the Landsat surface reflectance available on Google Earth Engine (GEE), the estimated TSM concentration values were calculated using the model fitted by the band reflectance and the TSM measurements at sampling points. First, we visually filtered and recorded the images covered by thin clouds according to Landsat Look Natural Color Image from the USGS (https://search.earthdata.nasa.gov/). Then, we automated cloud cover threshold (<60%) control and date control (excluding images covered by thin clouds) using GEE via its python API. We used all the scenes with a cloud cover threshold of less than 60% and without the thin clouds covering the study area in this calculation every year (May to October, 1984–2019). The clouds/cloud shadow/ice influenced pixels were further automatically removed according to the pixel quality assessment (pixel_qa) band. Nonwater masking was performed automatically by a fixed threshold of certain bands or bands combinations, such as normalized difference water index [NDWI: (green-NIR)/(green+NIR)] and modified NDWI [MNDWI: (green-SWIR)/(green+SWIR)]. The pixels whose average of NDWI and MNDWI less than 0.15 were masked out. Finally, the arithmetic average of all good scenes in the same place was derived annually as the annual TSM value using a python-based processor available on GEE (https://code.earthengine.google.com/). In total, the TSM concentrations dataset derived from Landsat data contains 36 annual TSM maps covering the study area in 1984–2019.

E. Ancillary Data and Processing

The digital elevation model (DEM) (http://www.resdc.cn), watershed data (http://www.geodata.cn), the soil erosion data (http://www.resdc.cn), soil type data (http://www.geodata.cn) and the ecosystem data (http://www.resdc.cn) (all of them are 1 km grid) were used. Moreover, annual precipitation data (1 km grid) (http://www.resdc.cn) and annual wind speed data (1 km grid) (http://www.geodata.cn) as the main meteorological factors, and annual NDVI data (http://www.gscloud.cn) were acquired and processed to generate their dynamic maps using an IDL program.

F. Analysis Methods

We analyze the TSM concentrations of the lakes by means of summary statistics in terms of annual mean value (ANN_{TSM}), changing rate (R), multiyear average value (AVG_{TSM}), and coefficient of variation (CV). First, each of the annual TSM maps generated from the Landsat product was spatially averaged using lake boundaries, so that we could obtain the time series of the annual mean TSM (ANN_{TSM}) for the lakes. Then, linear regressions were performed among the annual values from the TSM time series (with TSM of more than ten years) to obtain the rates of change (R) in TSM during the study period (4). The average values of the multi-year TSM (AVG_{TSM}) were calculated according to (5). The CV was calculated according
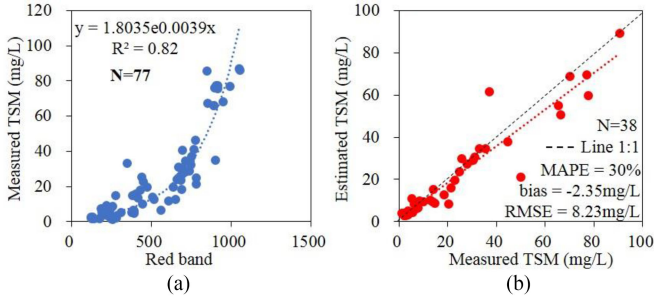
Fig. 2. Scatter plots of calibration and validation for TSM retrieval model. (a) Model calibration. (b) Model validation.

to (6) and (7). The calculation formulas were expressed as

$$R = \frac{\sum (ANN_{TSM} - \overline{ANN_{TSM}})(y - \bar{y})}{\sum (ANN_{TSM} - \overline{ANN_{TSM}})^2} \quad (4)$$

$$AVG_{TSM} = \frac{\sum ANN_{TSM}}{N} \quad (5)$$

$$CV = \frac{SD}{AVG_{TSM}} \times 100\% \quad (6)$$

$$SD = \sqrt{\frac{\sum (ANN_{TSM} - AVG_{TSM})^2}{N}} \quad (7)$$

where "y" was the year ranging from 1 to 36 (replaces 1984 to 2019); "N" was the number of years ranging from 1 to 36.

The histograms or percentage of these indicators were generated to determine the characteristics of the TSM dynamics. The correlations between the annual TSM series and the corresponding wind speed, precipitation and NDVI series were obtained based on the Spearman correlation analysis.

III. RESULTS

A. TSM Retrieval Model

The *in situ* TSM exhibited a wide range of TSM concentrations (range: 1.2–860 mg/L, mean: 56.7 mg/L) and significant differences among samples [standard deviation (SD) was 126.8 mg/L]. There was a statistical significant correlation between the reflectance of red band from Landsat surface reflectance data and the TSM concentrations. Further, there was a more stable exponential function relationship between them [see Fig. 2(a)]. The exponential function was validated and assessed to be a more feasible option for TSM retrieval in the study area relative to other models (see Fig. S1). The determination coefficient (R^2) of this model calibration was 0.82 [see Fig. 2(a)], and the RMSE, MAPE and bias between the measured TSM and the estimated TSM was 8.23 mg/L, 30% and −2.35 mg/L, respectively [see Fig. 2(b)]. The validation points of this model were also reasonably distributed along the 1:1 line [see Fig. 2(b)].

B. TSM Spatiotemporal Dynamics

Fig. 3 showed the annual TSM concentrations series for 591 lakes from 1984 to 2019. The color variations in Fig. 3 indicated
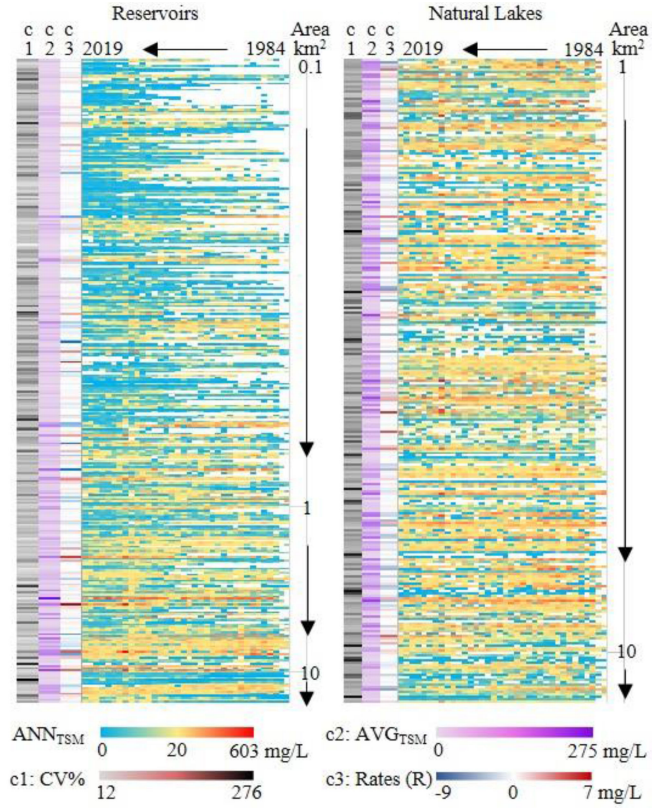

Fig. 3. Annual TSM and its dynamics of 591 lakes across Inner Mongolia. Note: Here lakes are natural lakes. ANNTSM is the annual TSM value. The "*R*" is the changing rate during 1984–2019. The AVGTSM is the arithmetic average of TSM during 1984–2019. The "CV" is the variation coefficient. Colorless blocks represent missing data.

the variations of TSM among lakes and years. Superimposed on the interannual variations for each lake were the significant spatial heterogeneities over the entire region. The annual TSM less than 20 mg/L appeared in most of the reservoirs, especially in those built after 2000 with an area of 0.1 to 1 km² (see Fig. 3). The annual TSM concentrations higher than 20 mg/L mostly occurred irregularly in the lakes with an area larger than 1 km² from 1984 to 2019, especially in the lakes with areas of 1 to 10 km² (see Fig. 3). The annual TSM concentrations of 591 lakes were divided into four levels (0–25 mg/L, 25–50 mg/L, 50–100 mg/L and >100 mg/L), the relative percentage of lakes with the TSM between 0–25 mg/L increased slightly from 1984–2019 and the percentage of lakes with TSM >100 mg/L decreased slightly (see Fig. S2). Tendency of the annual TSM series over the 36-year observation period revealed that TSM concentrations decreased in some lakes [dark blue blocks of the third column (c3) in Fig. 3], while increased in other lakes [dark red blocks of the third column (c3) in Fig. 3]. In the period of 1984–2019, the CV of TSM concentrations in the lakes was between 12%–276%. The TSM concentrations were relatively stable in some lakes (with lower CV values), while less stable in other lakes (with higher CV values) [the first column (c1) in Fig. 3]. For example, the CV of TSM concentrations in 6 natural lakes with an area greater than 10 km² was greater than 135mg/L, which
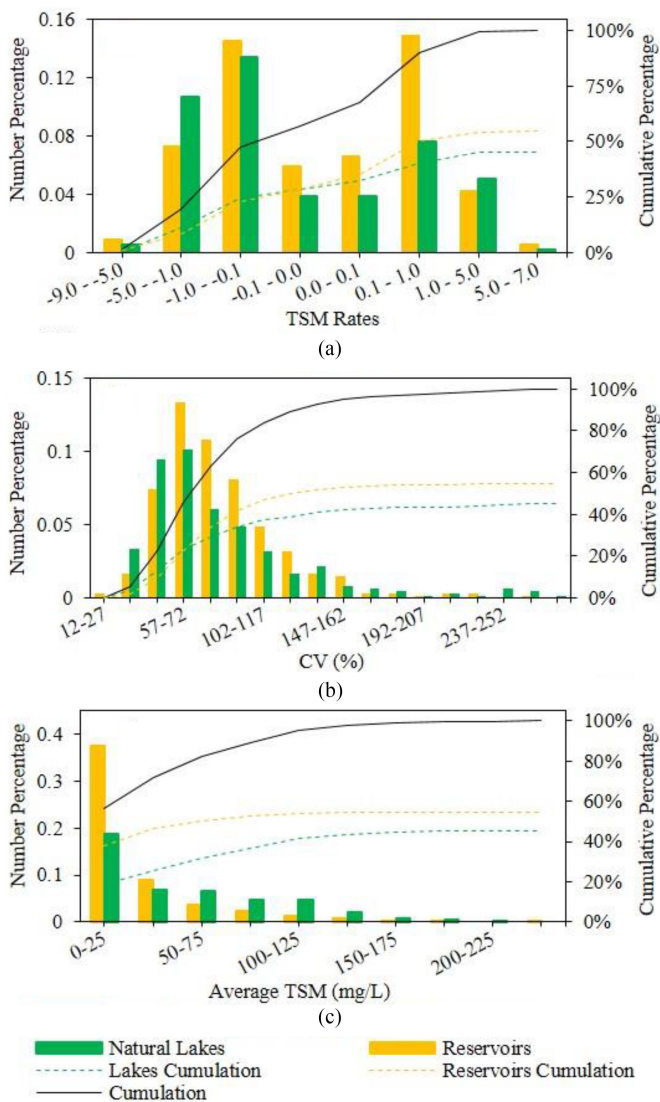
Fig. 4. (a) Histogram of the TSM changing rates. (b) Histogram of the CV of annual TSM. (c) Histogram of the average TSM. Note: green bars represent lakes and orange bars represent reservoirs; The black solid line represents the cumulative percentage of all lakes and reservoirs, the green dashed line represents the cumulative percentage of lakes and the orange dashed line represents the cumulative percentage of reservoirs.

Fig. 5. Spatial distribution of 36-year average TSM (1984 to 2019).
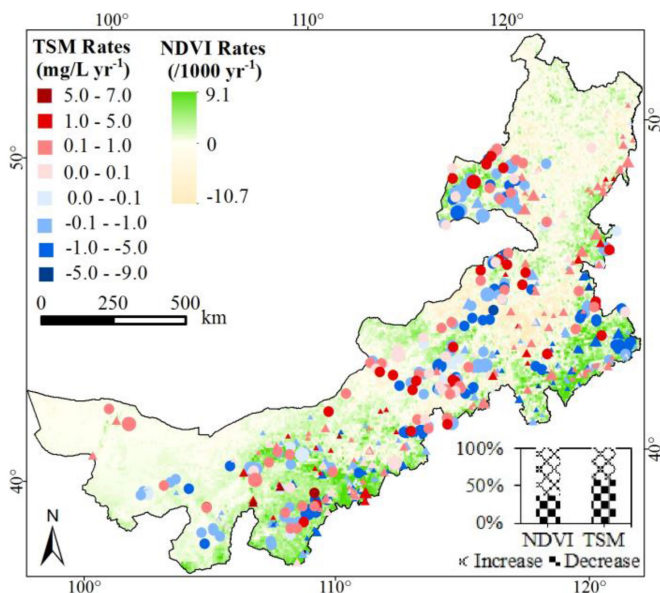
Fig. 6. Changing rates of annual NDVI and annual TSM in the study area. Note: Rates is the changing rates (the same below). Triangles or circles with different sizes represent different types of lakes and their area levels (as shown in Fig. 5).

was extremely unstable. The higher and lower values of the 36-year average TSM occurred in lakes with different levels of area [the second column (c2) in Fig. 3]. Overall, the average TSM concentrations in the lakes varied from 0 to 275 mg/L.

The changing rates (also see in Fig. 3) were summarized in Fig. 4(a). Overall, the annual TSM concentrations decreased in 57.02% of the lakes, while increased in 42.98% of the other lakes (also see in Fig. 5). Obviously, among the eight levels of changing rates, the percentage of lakes with a changing rate between -0.1 and -1 mg/L/yr was the highest (27.92%), followed by another 22.5% of lakes with a changing rate between 0.1 and 1 mg/L/yr [see Fig. 4(a)]. The number of lakes (green bars) showing a decrease in annual TSM concentration was more than that of reservoirs (orange bars), and conversely, the number of

reservoirs showing an increase in annual TSM was more than that of lakes [see Fig. 4(a)]. The distributions of TSM changing rates in each lake were clearly displayed in Fig. 6.

The CV of the annual TSM concentrations in the lakes from 1984 to 2019 were summarized in Fig. 4(b), reflecting the interannual variability of the TSM concentration. The CV of TSM concentrations in 75.8% of the lakes was within 102% and in 24.2% of the lakes was above 102% [see Fig. 4(b)]. The percentage of lakes with the CV between 57%–72% was the highest (23.5%) and the percentages of lakes with the CV above

72% or below 57% were decreased [see Fig. 4(b)]. Furthermore, the number of lakes (green bars) was slightly more than that of reservoirs (orange bars) when the CV of TSM concentrations was below 72%, while the number of reservoirs obviously exceeded lakes when the CV was above 72% [see Fig. 4(b)].

The 36-year TSM average results for all lakes were shown in the map of Fig. 5 (see Fig. 3), and the spatial patterns of the TSM distributions could be clearly observed. It was seen that the TSM concentrations in most reservoirs were less than 50 mg/L and in most natural lakes were more than 50 mg/L. Similar to the Fig. 3, of the 591 lakes, 56.18% (37.56% are reservoirs) were relatively clear with long-term averaged TSM concentrations below 25 mg/L, 15.74% were relatively turbid with long-term averaged TSM concentrations between 25–50 mg/L, 17.26% were more turbid with long-term averaged TSM concentrations between 50–100 mg/L and 10.83% were very turbid with long-term averaged TSM concentrations above 100 mg/L [see Fig. 4(c)].

C. Environmental Factors Versus TSM

The TSM in the examined lakes demonstrated spatiotemporal variations as expected. As the main influence factors, the vegetation, wind speed and precipitation [27], [28] were analyzed. As a result, the vegetation represented by NDVI across the study area indicated strong variation characteristics (see Fig. 6). Overall, 63.76% of NDVI was increasing and 36.24% was decreasing. Meanwhile, the TSM in 57.02% of the lakes were decreasing and in 42.98% of the lakes were increasing (see Fig. 6). This indicated that the large-scale increase in NDVI was accompanied by a significant decrease in TSM of lakes. Specifically, the TSM of some lakes changed in the same direction as the NDVI around them, and the TSM and the NDVI changed in reverse for other lakes (see Fig. 6).

The dynamics of NDVI and TSM were calculated by superimposing the environmental backgrounds (watersheds (see Fig. S4), ecosystems (see Fig. S5), soil types (see Fig. S6) and soil erosion types (see Fig. S7) that might affect TSM. The results showed that the overall TSM dynamics and NDVI dynamics based on different regions both showed regional differences (see Fig. 7). For the watersheds, the NDVI decreased in five watersheds (orange in Fig. 7) and increased in the other 20 watersheds (green in Fig. 7), while the TSM decreased in 19 watersheds (blue in Fig. 7) and increased in the other six watersheds (red in Fig. 7). The TSM and NDVI was significantly negatively correlated in 4 watersheds (see Fig. 7). For the ecosystems, the NDVI decreased in the forest ecosystem region and increased in the other ecosystems, while the TSM increased in all these ecosystem regions (see Fig. 7). The TSM and NDVI was significantly negatively correlated in the forest ecosystem region (see Fig. 7). For the soil types, the NDVI increased in all the soil type regions, while the TSM decreased in the clay and sand regions and increased in the other soil type regions (see Fig. 7). The TSM and NDVI was significantly negatively correlated in the sand region (see Fig. 7). For the soil erosion regions, the NDVI decreased in only two soil erosion-type regions and increased in the other 11 regions, while the TSM increased in nine soil erosion type regions and decreased only in four regions. The TSM
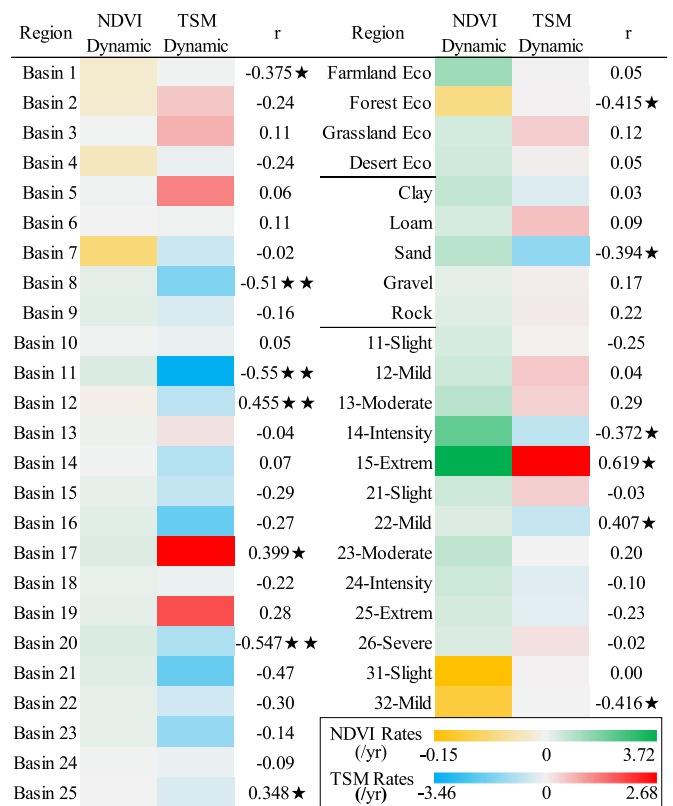
Region	NDVI Dynamic	TSM Dynamic	r	Region	NDVI Dynamic	TSM Dynamic	r
Basin 1			-0.375 ★	Farmland Eco			0.05
Basin 2			-0.24	Forest Eco			-0.415 ★
Basin 3			0.11	Grassland Eco			0.12
Basin 4			-0.24	Desert Eco			0.05
Basin 5			0.06	Clay			0.03
Basin 6			0.11	Loam			0.09
Basin 7			-0.02	Sand			-0.394 ★
Basin 8			-0.51 ★★	Gravel			0.17
Basin 9			-0.16	Rock			0.22
Basin 10			0.05	11-Slight			-0.25
Basin 11			-0.55 ★★	12-Mild			0.04
Basin 12			0.455 ★★	13-Moderate			0.29
Basin 13			-0.04	14-Intensity			-0.372 ★
Basin 14			0.07	15-Extrem			0.619 ★
Basin 15			-0.29	21-Slight			-0.03
Basin 16			-0.27	22-Mild			0.407 ★
Basin 17			0.399 ★	23-Moderate			0.20
Basin 18			-0.22	24-Intensity			-0.10
Basin 19			0.28	25-Extrem			-0.23
Basin 20			-0.547 ★★	26-Severe			-0.02
Basin 21			-0.47	31-Slight			0.00
Basin 22			-0.30	32-Mild			-0.416 ★
Basin 23			-0.14				
Basin 24			-0.09				
Basin 25			0.348 ★				

NDVI Rates (/yr) -0.15 0 3.72
TSM Rates (/yr) -3.46 0 2.68

Fig. 7. Changing rates of annual TSM and annual NDVI based on different environmental background regions. Note: The symbol "★" ("★★") represents significant correlations ($p < 0.05$ (0.01)). "*r*" represents correlation coefficient between annual TSM and annual NDVI from 1984 to 2019. The words "clay-rock" represent different soil types. "farmland eco-desert eco" represent different ecosystems. "11–15" represent different levels of water erosion; "21–26" represent different levels of wind erosion; "31"and "32" represent different levels of freeze-thaw erosion.

and NDVI was significantly negatively correlated in two soil erosion regions (see Fig. 7). In addition, the scatter plots between the annual NDVI and the annual TSM for these environmental background regions showed that the NDVI value was higher, the TSM was generally lower and more stable in most region (see Fig. S3). For example, the NDVI value of the forest ecosystem region was generally high while its TSM value was relatively low and not very scattered [see Fig. S3(b)]. The percentage of the lakes located in different environmental background regions with different tendency of TSM were clearly displayed in Fig. S4–S7. It could be seen that the TSM increased in some lakes and decreased in the other lakes for each basin (except basin 25), each ecosystem region, each soil type region, and each soil erosion region.

Similar to the TSM variations, the meteorological factors in the study area also demonstrated interannual variations and regional differences (see Fig. 8). Overall, precipitation had decreased in most regions (except in the western region) of the study area [see Fig. 8(a)]. Wind speed had declined in the eastern, western and a small part of the northwest regions, and had increased in the central and northern regions [see Fig. 8(b)]. Furthermore, the correlations between annual TSM and corresponding local wind and precipitation were examined using the
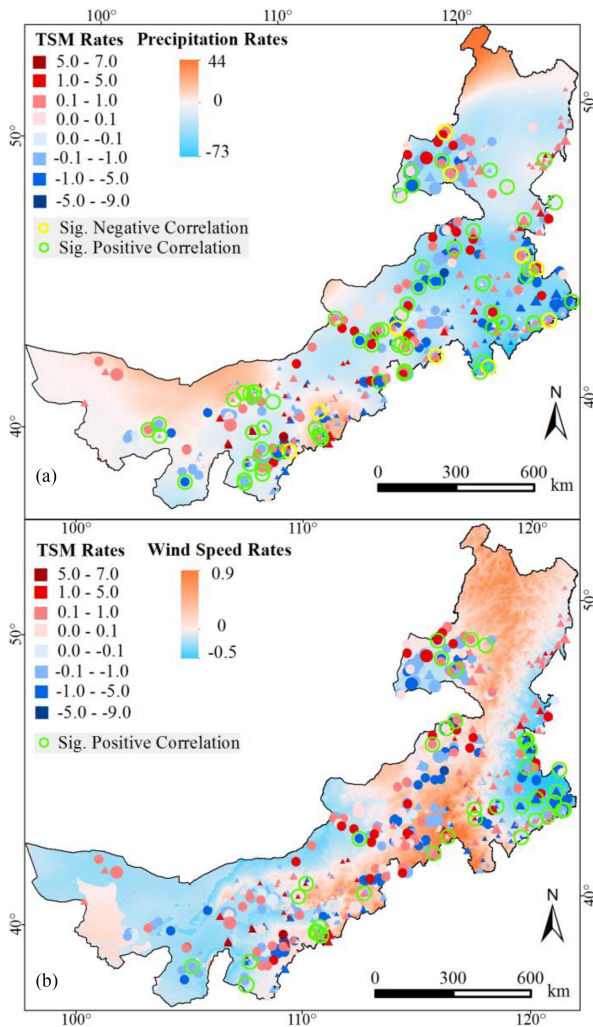
Fig. 8. Spatial distributions of the changing rates for TSM and Meteorological factors. (a) For the precipitation and TSM. (b) For the wind speed and TSM. Note: The TSM in the lakes circled by the yellow circle was significantly negatively correlated with precipitation. The TSM in the lakes circled by the green circle was significantly positively correlated with precipitation. Triangles or circles with different sizes represent different types of lakes and their area levels (as shown in Fig. 5).

Fig. 9. Percentage of the number of lakes in different levels of correlation coefficients (r) between annual TSM and meteorological factors. (a) For the "r" between precipitation and TSM. (b) For the "r" between wind speed and TSM.

Spearman correlation analysis for each lake (see Fig. 9). We found both positive and negative correlations for the 591 lakes, suggesting that the effects of these factors on the TSM varied for different lakes. According to statistics, the precipitation was negatively correlated with the TSM in 35.84% of the lakes, and was positively correlated with the TSM in the other lakes. The significant effect ($p < 0.05$) displayed merely in 12.8% of the lakes [see Fig. 9(a)]. The positive and negative correlations between TSM and precipitation were reflected in both lakes [green bars in Fig. 9(a)] and reservoirs [orange bars in Fig. 9(a)]. According to our statistics, the TSM in 42.47% of the lakes was positively correlated with the wind speed and in 6.6% of the lakes was significantly positively correlated [see Fig. 9(b)]. In addition, the positive correlations between TSM and wind speed were mainly reflected in lakes (green bars in Fig. 9(b)). For each lake, the details of the relationships between TSM and precipitation or wind speed were presented in the superimposed
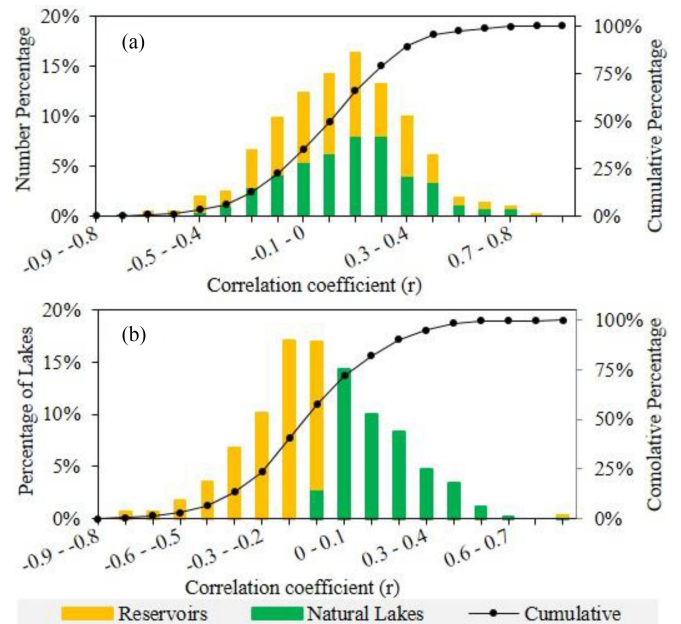
maps of the two in Fig. 8. The lakes where TSM was significantly related to these two meteorological factors could be clearly seen in Fig. 8 (lakes circled by the yellow and green circle).

IV. DISCUSSION

A. Assessment of the Landsat-Based Model

While the atmospheric corrections used to generate these surface reflectance products were originally developed for terrestrial applications, a growing body of research shows that they can be used to accurately estimate inland water quality parameters [29], [30] and perform on par with water-specific atmospheric correction algorithms [31]. The Landsat surface reflectance product (from LEDAPS and LaSRC) have been used to estimate chlorophyll, clarity and CDOM in lakes, reservoirs and rivers at different reginal scales [29], [32]–[34]. TSM is the first water quality parameter researched by remote sensing, so a lot of research has been done on it with the Landsat surface reflectance products [15], [35], [36] which are more adequate for TSM than other parameters. In addition, the relationship between the Landsat surface reflectance product and the measured TSM performed well ($R^2 = 0.82$). Calculating the validation error metrics using the random validation data set data ($n = 38$) can reaffirm the sensor correction procedure [31]. The validation metrics for the TSM retrieval model showed the RMSE of 8.23 mg/L, MAPE of 30% and bias of -2.35 mg/L. As an additional test, we compared the in-situ reflectance from some water bodies to the Landsat surface reflectance product, and the results showed that both types of reflectance values displayed similar variation trends at the different wavelengths (see Fig. S8). And the reflectance from the Landsat 8 product were consistent to the in situ measured reflectance values and the uncertainty

levels in visible bands (blue: 39.81%, green: 9.02%, and red: 0.2%) could be acceptable according to previous studies [30], especially the red band. Thus, the Landsat surface reflectance products can be used for remote sensing estimations of TSM in the study area.

Previous studies have shown that red spectra-based models can be used to estimate water transparency and the related parameters such as turbidity and TSM concentration with good accuracy in moderately turbid lakes/reservoirs and coastal lakes [27], [28], [37]. Using the red spectra as a reference band could obtain reasonable accuracy in deriving water transparency and the related parameters [30], [38], [39]. Our results of model validation showed that the accuracy of derived TSM based on the red band model was reasonable (RMSE was 8.23 mg/L, MAPE was 30% and bias was −2.35 mg/L) and better than other models (see Fig. S1). The red band model based on the Landsat was suitable for the TSM estimation. The experience learned from this study could be used in many current or future earth resources satellite data (such as Sentinel 2, Gao-Fen series, HJ A/B, and Landsat 9 which equipped with red band) to derive spatial and temporal TSM distributions in the study area.

Regrettably, due to the limitation of time, funding, geographical conditions and navigation conditions, not all water bodies were sampled (even for a certain lake, it is difficult to sample each part) in this article. Fortunately, by establishing a robust model, we can use remote sensing images for large-scale spatiotemporal water monitoring based on limited sample [27], [40], [41]. Bio-optical model is the tool that connects the satellite imagery to optical, biogeochemical, and water quality parameters [33] and its robustness depends on the samples. In other words, the robustness of the model can reflect the quality (representativeness) of the samples. The validation results suggested that the model developed for retrieving TSM in the study area was robust, with the calibration R^2 of 0.82 [see Fig. 2(a)], the RMSE of 8.23 mg/L, MAPE of 30% and bias of -2.35 mg/L. As an additional test, a total of 117 additional water samples from the water bodies near the study area (see Table S2) were collected and used to further test the model. The test results were good according to previous research [15], [27], [36] with RMSE of 11.67 mg/L, MAPE of 0.18 and bias of -2.68 (see Fig. S9), confirming that the model based on these samples (115) can be used to all the water in the study area. It is confirmed that the model based on these samples (115) can be used to all the water in the study area.

To evaluate the consistency of the Landsat series images, the minor differences in the spectral response of sensors used across Landsat missions has been compared by previous studies [30]–[32], [34]. Their comparison results indicated that the agreement of the reflectance between Landsat sensors (5 versus 7 and 7 versus 8) was very strong, especially in the red band. This means that the model using the red band from Landsat is generalizable from 1984–2019 between Landsat sensors. In addition, our additional test results for the additional samples (most of them were synchronized with Landsat 5 TM) (see Table S2 and Fig. S9) also confirmed that our model is generalizable from 1984–2019 between Landsat sensors. Thus, the use of Landsat series data with the proposed model can provide accurate long-term coverage of TSM in water bodies across the study area.

B. Assessment of Retrieval Results

Because of the optical variability in lakes, TSM concentrations retrieved from remote sensing data might be underestimated or overestimated compared to monitoring station measurement [34], [36]. The wide distribution of our samples (see Fig. 1) and the range of TSM concentrations (from 1.2 to 860 mg/L, SD was 126.87 mg/L) represented the water with different turbidity, and the model developed for TSM retrieval was robust [see Fig. 2(b)], so this error could be minimized as much as possible. In addition, the quality of the image itself might introduce some errors in the estimation of the TSM concentration in lakes [15]. The image quality was greatly improved by cloud control, cloud removal and land mask processing, reducing the impact on TSM estimation.

To fully cover the land surface area of the study area, about 78 Landsat images are needed. Due to the lack of images caused by data storage and quality control (cloud filtering), there was difference in the number of images each year. And 95–594 images were used in each year (see Fig. S10). As an additional test, we compared the TSM (calculated by different methods) in six lakes during 2015–2019. As a result, the annual mean TSM calculated based on the daily images and based on the seasonal mean TSM showed a difference in some lakes (see Fig. S11). It is demonstrated that the annual mean TSM might be affected by the inconsistent number of effective images in different seasons. If the annual mean TSM was calculated based on the seasonal mean TSM, the result might be more accurate.

The possible errors in the TSM values due to some inevitable reasons were reduced by climatologically and spatially averaging. We obtained the annual values by averaging the multi-period TSM concentration data, thus some over- or under-estimated values might be offset. Attila *et al.* [55] found that the chlorophyll-a statistics calculated for a given water body by spatially averaging can represent the water body well [42]. Likewise, the TSM concentration statistics calculated for a given water body should be suitable for understanding the quality of the lakes. This is suitable for the research that serves to formulate water management strategies on a regional scale.

In the long-term research of water transparency by Liu *et al.* [52], the transparency in seven lakes (area > 20 km^2) across Inner Mongolia decreased and in seven lakes increased from 2000 to 2018. The TSM in 10 lakes among the 19 lakes with area >20 km^2 detected in our research decreased and in nine lakes increased during the same period (2000–2018). The tendency of water transparency in some lakes was contrary to the tendency of TSM, while in some lakes their relationship in tendency is another phenomenon. This indicated that different data sources (MODIS and Landsat) might affect the analysis tendency of water quality due to their differences in time resolution.

C. Impacts of Environmental Factors on TSM Variations

The analysis of the relationship between NDVI and TSM could be used to study the possible explanations of NDVI to

the annual TSM change of most lakes. However, TSM changes in some lakes might not be explained by NDVI. For example, the increased TSM in some lakes in the 8th watershed could not be explained by the increased NDVI. In practice, a specific water body should be paid more attention to take an appropriate measure to improve vegetation information.

We explored the impact of other potential factors on the role of NDVI. In the results of Spearman correlation analysis (see Fig. 7), the positive correlation between NDVI and TSM demonstrated that the effect of NDVI on TSM changes was interfered (or even obliterated) by other factors. For those watersheds with a positive correlation (see Fig. 7), if the weak NDVI change was not the reason, then the most plausible cause of TSM change was the topography (DEM see Fig. S4) reflecting the characteristics of the watershed. For example, the decreased TSM of the sixth and tenth basins were not caused by the increased NDVI, but probably due to the lower elevation beneficial to soil and water conservation. For the 14th and 25th basins with the same situation, the elevation (higher) might not be a reasonable explanation for the TSM changes, and it was more likely to be attributed to other factors. The increased NDVI of the farmland ecosystem region did not promote the decrease in TSM (see Fig. 7), probably because of the overall improvement of crops in recent years, had also been accompanied by an increase in negative human impacts (such as fertilizer use and soil loosening) [43], [44]. The situation of the grassland ecosystem implied that TSM might be affected by grazing activities (the suspended solids were disturbed by the arrival of livestock) [45], [46]. The increased NDVI of the desert ecosystem in the western region has benefited significantly from the projects "reverting farmland to forests" and "afforestation" launched by the Chinese government at the end of the 20th century [47]. In contrast, the TSM changes in this region were not ideal, which might be related to the bad weather events (sand storms or flood) [48], [49]. TSM changes of other soil types regions (except for the sand region) (see Fig. 7) might be affected by human activities and the soil texture, for example, the decreased TSM of the clay region might be mainly caused by the poor water permeability (not easy to lose with runoff) of this soil type [44], [50]. Finally, the correlation coefficient "r" of the soil erosion types (see Fig. 7) showed that the role of vegetation represented by NDVI on the TSM for the 6 soil erosion regions was interfered by other factors (might be wind erosion, precipitation erosion or freeze-thaw erosion effect) [51].

In summary, the effect of the factors (NDVI, wind speed and precipitation) on the TSM change was not always exposed, because it might be weakened or obliterated by others. It remains a challenge to accurately identify the factor that weakens or smears because multiple factors coexist in the TSM changes. Nevertheless, a comprehensive analysis of the factors surrounding the lakes certainly helps to determine the possible trends (better or worse) of its TSM variation.

V. CONCLUSION

For the first time, the 36-years TSM dynamics of the lakes across inner Mongolia were obtained using remote sensing technique. The model based on Landsat red band performed well with the calibration R^2 of 0.82, RMSE of 8.23 mg/L, MAPE of 30% and bias of -2.35 mg/L. The retrieved results revealed significant differences in the TSM variations for the 591 lakes. In the annual series, the TSM less than 20 mg/L mainly appeared in the reservoirs. The percentage of lakes with the TSM between 0–25 mg/L increased slightly from 1984–2019 and the percentage of lakes with TSM >100 mg/L decreased slightly. The 43.82% of the 591 lakes were relatively turbid with long-term averaged TSM above 25 mg/L. The TSM in all lakes was changing with different CV. The TSM in 42.98% of the lakes increased and in 57.02% of the lakes decreased. The number of natural lakes showing a decrease in TSM was more than that of reservoirs. Our study proved the importance of remote sensing observations in gathering large-scale water quality information, and the results obtained here should provide critical basics to support water quality management. Whilst the vegetation generally affected the TSM changes for most lakes, its role might be weakened or smeared due to the coexistence of other factors. Additionally, wind speed, precipitation, human activities (farming, grazing and construction), and soil texture also affected TSM changes for some lakes. In practice, comprehensive analysis on multiple factors is necessary. Particularly, the application of the similar sensors or more advanced sensors would assist constructing consistent and more complete satellite-derived time series data. The overall analysis of TSM dynamics here should help making macro-level decisions on water quality management. In practice, specific treatment and protection plans should also be formulated for a specific water.

REFERENCES

[1] N. Pahlevan, S. K. Chittimalli, S. V. Balasubramanian, and V. Vellucci, "Sentinel-2/Landsat-8 product consistency and implications for monitoring aquatic systems," *Remote Sens. Environ.*, vol. 220, pp. 19–29, Jan. 2019.

[2] H. W. Paerl and V. J. Paul, "Climate change: Links to global expansion of harmful cyanobacteria," *Water Res.*, vol. 46, no. 5, pp. 1349–1363, Apr. 2012.

[3] A. M. Michalak *et al.*, "Record-setting algal bloom in lake erie caused by agricultural and meteorological trends consistent with expected future conditions," *Proc. Nat. Acad. Sci. United States Amer.*, vol. 110, no. 16, pp. 6448–6452, Apr. 2013.

[4] K. P. Singh, A. Malik, D. Mohan, and S. Sinha, "Multivariate statistical techniques for the evaluation of spatial and temporal variations in water quality of Gomti river (India) - a case study," *Water Res.*, vol. 38, no. 18, pp. 3980–3992, Nov. 2004.

[5] A. Qadir, R. N. Malik, and S. Z. Husain, "Spatio-temporal variations in water quality of nullah Aik-tributary of the river Chenab, Pakistan," *Environ. Monit. Assessment*, vol. 140, no. 1–3, pp. 43–59, May 2008.

[6] B. Zhang, J. Li, Q. Shen, and D. Chen, "A bio-optical model based method of estimating total suspended matter of lake Taihu from near-infrared remote sensing reflectance," *Environ. Monit. Assessment*, vol. 145, no. 1–3, pp. 339–347, 2008.

[7] M. J. Paul and J. L. Meyer, "Streams in the urban landscape," in *Urban Ecology*, Berlin, Germany: Springer, 2008, pp. 207–231.

[8] E. Alcantara, M. Curtarelli, and J. Stech, "Estimating total suspended matter using the particle backscattering coefficient: Results from the itumbiara hydroelectric reservoir (Goias state, brazil)," *Remote Sens. Lett.*, vol. 7, no. 4, pp. 397–406, 2016.

[9] L. Feng, X. J. Hou, and Y. Zheng, "Monitoring and understanding the water transparency changes of fifty large lakes on the yangtze plain based on long-term MODIS observations," *Remote Sens. Environ.*, vol. 221, pp. 675–686, Feb. 2019.

[10] D. Blondeau-Patissier, J. F. R. Gower, A. G. Dekker, S. R. Phinn, and V. E. Brando, "A review of ocean color remote sensing methods and statistical techniques for the detection, mapping and analysis of phytoplankton blooms in coastal and open oceans," *Prog. Oceanogr.*, vol. 123, pp. 123–144, Apr. 2014.

[11] P. J. Werdell *et al.*, "An overview of approaches and challenges for retrieving marine inherent optical properties from ocean color remote sensing," *Prog. Oceanogr.*, vol. 160, pp. 186–212, 2018.

[12] N. Pahlevan, Z. P. Lee, J. W. Wei, C. B. Schaaf, J. R. Schott, and A. Berk, "On-orbit radiometric characterization of OLI (Landsat-8) for applications in aquatic remote sensing," *Remote Sens. Environ.*, vol. 154, pp. 272–284, Nov. 2014.

[13] V. Quinten and R. Kevin, "Atmospheric correction of metre-scale optical satellite data for inland and coastal water applications," *Remote Sens. Environ.*, vol. 216, pp. 586–597, 2018.

[14] Y. Oyama, B. Matsushita, T. Fukushima, K. Matsushige, and A. Imai, "Application of spectral decomposition algorithm for mapping water quality in a turbid lake (Lake kasumigaura, japan) from landsat TM data," *ISPRS J. Photogramm. Remote Sens.*, vol. 64, no. 1, pp. 73–85, Jan 2009.

[15] Y. X. Du *et al.*, "Quantifying total suspended matter (TSM) in waters using landsat images during 1984-2018 across the songnen plain, northeast china," *J. Environ. Manage.*, vol. 262, May 2020, Art. no. 110334.

[16] T. Lacava *et al.*, "A MODIS-based robust satellite technique (RST) for timely detection of oil spilled areas," *Remote Sens.*, vol. 9, no. 2, pp. 1–15, Feb 2017.

[17] D. Zhang, S. Lavender, J. P. Muller, D. Walton, X. Zou, and F. Shi, "MERIS observations of phytoplankton phenology in the baltic sea," *Sci. Total Environ.*, vol. 642, no. 15, pp. 447–462, 2018.

[18] J. E. O'Reilly and P. J. Werdell, "Chlorophyll algorithms for ocean color sensors-OC4, OC5 & OC6," *Remote Sens. Environ.*, vol. 229, pp. 32–47, Aug. 2019.

[19] G. Liu *et al.*, "A four-band semi-analytical model for estimating phycocyanin in inland waters from simulated MERIS and OLCI data," *IEEE Trans. Geosci. Remote Sens.*, vol. 56, no. 3, pp. 1374–1385, Mar 2018.

[20] E. Ciancia *et al.*, "Investigating the chlorophyll-a variability in the gulf of taranto (North-western ionian sea) by a multi-temporal analysis of MODIS-Aqua level 3/level 2 data," *Continental Shelf Res.*, vol. 155, pp. 34–44, 2018.

[21] A. Gitelson, G. Garbuzov, F. Szilagyi, K. H. Mittenzwey, A. Karnieli, and A. Kaiser, "Quantitative remote-sensing methods for real-time monitoring of inland waters quality," *Int. J. Remote Sens.*, vol. 14, no. 7, pp. 1269–1295, May 1993.

[22] Z. Y. Lu *et al.*, "Modification of 6SV to remove skylight reflected at the air-water interface: Application to atmospheric correction of landsat 8 OLI imagery in inland waters," *Plos One*, vol. 13, no. 8, Aug 2018, Art. no. e0202883.

[23] M. H. Wang, "The rayleigh lookup tables for the SeaWiFS data processing: Accounting for the effects of ocean surface roughness," *Int. J. Remote Sens.*, vol. 23, no. 13, pp. 2693–2702, 2002.

[24] M. S. Moran *et al.*, "A refined empirical line approach for reflectance factor retrieval from landsat-5 TM and landsat-7 ETM+," *Remote Sens. Environ.*, vol. 78, no. 1/2, pp. 71–82, Oct 2001.

[25] D. Schlapfer, A. Hueni, and R. Richter, "Cast shadow detection to quantify the aerosol optical thickness for atmospheric correction of high spatial resolution optical imagery," *Remote Sens.*, vol. 10, no. 2, Feb 2018.

[26] H. M. Gao, "Countermeasures of water resources supply and demand for inner Mongolia," Beijing: Chinese Academy of Agricultural Sciences, pp. 1–43, Nov. 2007.

[27] K. Shi *et al.*, "Long-term remote monitoring of total suspended matter concentration in lake taihu using 250 m MODIS-Aqua data," *Remote Sens. Environ.*, vol. 164, pp. 43–56, Jul. 2015.

[28] X. J. Hou, L. Feng, H. T. Duan, X. L. Chen, D. Y. Sun, and K. Shi, "Fifteen-year monitoring of the turbidity dynamics in large lakes and reservoirs in the middle and lower basin of the yangtze river, china," *Remote Sens. Environ.*, vol. 190, pp. 107–121, Mar. 2017.

[29] C. Kuhn *et al.*, "Performance of landsat-8 and sentinel-2 surface reflectance products for river remote sensing retrievals of chlorophyll-a and turbidity," *Remote Sens. Environ.*, vol. 224, pp. 104–118, Apr. 2019.

[30] Y. Zhang, Y. Zhang, K. Shi, Y. Zhou, and N. Li, "Remote sensing estimation of water clarity for various lakes in China," *Water Res.*, vol. 192, 2021, Art. no. 116844.

[31] S. N. Topp, T. M. Pavelsky, E. H. Stanley, X. Yang, C. G. Griffin, and M. R. V. Ross, "Multi-decadal 1 improvement in U.S. lake water clarity," *Environ. Res. Lett.*, vol. 16, 2021, Art. no. 055025.

[32] J. R. Gardner, X. Yang, S. N. Topp, M. R. V. Ross, E. H. Altenau, and T. M. Pavelsky, "The color of rivers," *Geophys. Res. Lett.*, vol. 48, no. 1, Jan. 2021, Art. no. e2020GL088946.

[33] C. G. Griffin, J. W. McClelland, K. E. Frey, G. Fiske, and R. M. Holmes, "Quantifying CDOM and DOC in major arctic rivers during ice-free conditions using landsat TM and ETM plus data," *Remote Sens. Environ.*, vol. 209, pp. 395–409, May 2018.

[34] K. S. Song *et al.*, "Quantification of lake clarity in china using landsat OLI imagery data," *Remote Sens. Environ.*, vol. 243, Jun 2020, Art. no. 111800.

[35] S. Imen, N. B. Chang, and Y. J. Yang, "Developing the remote sensing-based early warning system for monitoring TSS concentrations in lake mead," *J. Environ. Manage.*, vol. 160, pp. 73–89, Sep 2015.

[36] C. Wang, S. Chen, D. Li, D. Wang, W. Liu, and J. Yang, "A Landsat-based model for retrieving total suspended solids concentration of estuaries and coasts in china," *Geoscientific Model Develop.*, vol. 10, pp. 4347–4365, 2017.

[37] S. Kratzer, C. Brockmann, and G. Moore, "Using MERIS full resolution data to monitor coastal waters - A case study from himmerfjarden, a fjord-like bay in the northwestern baltic sea," *Remote Sens. Environ.*, vol. 112, no. 5, pp. 2284–2300, May 2008.

[38] B. Nechad, K. G. Ruddick, and Y. Park, "Calibration and validation of a generic multisensor algorithm for mapping of total suspended matter in turbid waters," *Remote Sens. Environ.*, vol. 114, no. 4, pp. 854–866, Apr. 2010.

[39] K. Alikas and S. Kratzer, "Improved retrieval of secchi depth for optically-complex waters using remote sensing data," *Ecolog. Indicators*, vol. 77, pp. 218–227, Jun. 2017.

[40] F. Gohin *et al.*, "Twenty years of satellite and in situ observations of surface chlorophyll-a from the northern bay of biscay to the eastern English channel. Is the water quality improving?," *Remote Sens. Environ.*, vol. 233, Nov. 2019, Art. no. 111343.

[41] I. Chawla, L. Karthikeyan, and A. K. Mishra, "A review of remote sensing applications for water security: Quantity, quality, and extremes," *J. Hydrol.*, vol. 585, Jun. 2020, Art. no. 124826.

[42] J. Attila *et al.*, "Applicability of earth observation chlorophyll-a data in assessment of water status via MERIS - With implications for the use of OLCI sensors," *Remote Sens. Environ.*, vol. 212, pp. 273–287, Jun. 2018.

[43] X. Z. Gao, W. Q. Ma, Y. Cui, R. F. Wang, and F. S. Zhang, "Changes of soil nutrient contents and input of nutrients in arable of china," *Plant Nutrition Fertilizer Sci.*, vol. 6, no. 4, pp. 363–369, 2000.

[44] A. Klik and J. Rosner, "Long-term experience with conservation tillage practices in austria: Impacts on soil erosion processes," *Soil Tillage Res.*, vol. 203, Sep. 2020, Art. no. 104669.

[45] Y. Li and J. Zhao, "Effects of overgrazing on ecological and environmental construction and measurement," *J. Desert Res.*, vol. 25, no. 3, pp. 404–408, 2005.

[46] Y. X. Wang and J. M. Cao, "How to solve the overgrazing problem in inner mongolia," *Green Econ.*, no. 7, pp. 58–64, 2007.

[47] Q. F. Niu *et al.*, "Ecological engineering projects increased vegetation cover, production, and biomass in semiarid and subhumid northern china," *Land Degradation Develop.*, vol. 30, no. 13, pp. 1620–1631, Aug. 2019.

[48] C. Ding *et al.*, "Quantifying the spatio-temporal patterns of dune migration near minqin oasis in northwestern china with time series of landsat-8 and sentinel-2 observations," *Remote Sens. Environ.*, vol. 236, Jan 2020, Art. no. 111498.

[49] M. G. Donat, A. L. Lowry, L. V. Alexander, P. A. O'Gorman, and N. J. N. C. C. Maher, "More extreme precipitation in the world's dry and wet regions," *Nat. Clim. Change*, vol. 6, pp. 508–513, 2017.

[50] H. W. Pi, D. R. Huggins, and B. Sharratt, "Wind erosion of soil influenced by clay amendment in the inland pacific Northwest, USA," *Land Degradation Develop.*, vol. 15, pp. 241–255, 2020.

[51] D. Pimentel, "Soil erosion: A food and environmental threat," *Environ. Develop. Sustain.*, vol. 8, no. 1, pp. 119–137, 2006.

[52] D. Liu, "Observations of water transparency in China's lakes from space," *Int. J. Appl. Earth Obs. Geoinformation*, vol. 92, pp. 1–11, Oct. 2020, Art. no. 102187.

[53] K. Song, G. Liu, Q. Wang, Z. Wen, and C. Fang, "Quantification of lake clarity in China using Landsat OLI imagery data," *Remote Sens. Environ.*, vol. 243, pp. 1–12, Jun. 2020, Art. no. 111800.

[54] Y. Zhang, K. Shi, Y. Zhou, "Remote sensing estimation of water clarity for various lakes in China," *Water Res.*, vol. 192, pp. 1–13, Mar. 2021, Art. no. 116844.

[55] J. Attila *et al.*, "Applicability of earth observation chlorophyll-a data in assessment of water status via MERIS - With implications for the use of OLCI sensors," *Remote Sens. Environ.*, vol. 212, pp. 273–287, Jun. 2018.

Yunxia Du received the B.S. and M.S. degrees in land resource management from Jilin University, Changchun, China, in 2010 and 2013, respectively. She is currently working toward the Ph.D. degree in cartography and geographic information system with the University of Chinese Academy of Sciences, Beijing, Beijing, China.

Since 2018, she was a Member of Water Environment Remote Sensing Group, Northeast Institute of Geography and Agroecology, Chinese Academy of Sciences, Beijing. Her research interest includes the remote sensing on water environment.

Kaishan Song received the M.S. degree in GIS and cartography from Northeast Normal University, Changchun, China, in 2002, and the Ph.D. degree in remote sensing application from Northeast Institute of Geography and Agroecology (IGA), Chinese Academy of Sciences (CAS), Changchun, in 2005.

He is currently a Full Professor for remote sensing of environment applications with IGA, CAS. His current research interests include bio-optical properties of inland waters, remote sensing of water quality, and impact of climatic and anthropogenic driving forces on water quality spatiotemporal variations with remotely sensed imagery data.

Qiang Wang received the B.S. and M.S. degrees in physical geography from Jilin Normal University, Siping, China, in 2011 and 2019, respectively.

He is currently with the Northeast Institute of Geography and Agroecology, Chinese Academy of Sciences, Changchun, China. His research interests include water color remote sensing and optical properties in optically complex water bodies.

Ge Liu received the B.S. degree in geographic science from Liaocheng University, Liaocheng, China, in 2011, and the Ph.D. degree in environmental remote sensing from Nanjing Normal University, Nanjing, China, in 2017.

He is currently with the Northeast Institute of Geography and Agricultural Ecology, Chinese Academy of Sciences, Changchun, China. His research interests include water color remote sensing and optical properties in optically complex water bodies.

Zhidan Wen received the B.S. degree in bioengineering from Northeast Forestry University, Harbin, China, in 2007, the M.S. degree in microbiology from Shenyang Agricultural University, Shenyang, China, in 2010, and the Ph.D. degree in environmental science and engineering from the Harbin Institute of Technology, Harbin, in 2014.

She is currently with the Northeast Institute of Geography and Agroecology, Chinese Academy of Sciences, Changchun. Her research interests include carbon cycle in water and greenhouse gas emissions from inland water bodies.

Yingxin Shang received the B.S. degree in environmental science from the Changchun University of Science and Technology, Changchun, China, in 2012, and the Ph.D. degree in cartography and geographic information system from the University of Chinese Academy of Sciences, Beijing, China, in 2020.

She is currently with the Northeast Institute of Geography and Agroecology, Chinese Academy of Sciences, Changchun. Her research interests include water color remote sensing and optical properties in optically complex water bodies.

Lili Lyu received the master's degree in inorganic chemistry from the College of Chemistry, Northeast Normal University, Changchun, China, in 2011. She is currently working toward the Ph.D. degree in cartography and geographic information system with the Northeast Institute of Geography and Agroecology, Chinese Academy of Sciences, Changchun.

Her research interests include inversion of water quality parameters, evaluation of water nutritional status, measurement of water optical parameters, data mining, etc.

Jia Du received the B.S. degree in geography science major and the M.S. degree in cartography and geographic information system from Northeast Normal University, Harbin, China, in 2004 and 2007, respectively, and the Ph.D. degree in cartography and geographic information system from the Northeast Institute of Geography and Agroecology, Chinese Academy of Sciences, Changchun, China, in 2010.

He is currently with the Northeast Institute of Geography and Agroecology, Chinese Academy of Sciences. His research interests include quantitative remote sensing, remote sensing monitoring of heat flux of surface water, and remote sensing monitoring of conservation tillage.

Sijia Li received the B.S. degree in geographic science from Jilin Normal University, Changchun, China, in 2012, and the Ph.D. degree in environmental science from Northeast Normal University, Changchun, in 2020.

She is currently with the Northeast Institute of Geography and Agroecology, Chinese Academy of Sciences, Changchun. Her research interests include eutrophication monitoring, water color remote sensing, and lake carbon cycle in optically complex water bodies.

Hui Tao received the B.S. and M.S. degrees in geographic information system from Yanbian University, Jilin, China, in 2015 and 2018, respectively. She is currently working toward the Ph.D. degree in cartography and geographic information system with the Northeast Institute of Geography and Agroecology, Chinese Academy of Sciences, Changchun, China.

Her research interests include water clarity and total suspended matter.

Baohua Zhang received the M.S. degree from Henan University, Kaifeng, China, in 1999, and the Ph.D. degree from the Chengdu Institute of Mountain Hazards and Environment, Chinese Academy of Sciences, Chengdu, China, in 2004, both in physical geography.

He is currently with the School of Geography and Environment, Liaocheng University, Liaocheng, China. His research interests include soil and land information system.

Xiang Wang received the B.S. degree in land resource management and the M.S. degree in soil hyper-spectral remote sensing from Northeast Agricultural University, Harbin, China, in 2016 and 2019, respectively.

He is currently with the Northeast Institute of Geography and Agricultural Ecology, Chinese Academy of Sciences, Changchun, China. His research interests include soil spectral classification using VNIR spectra and soil properties prediction and mapping.